ISSN 1070-3632, Russian Journal of General Chemistry, 2010, Vol. 80, No. 3, pp. 604–617. © Pleiades Publishing, Ltd., 2010.
Original Russian Text © V.K. Ivanov, O.S. Polezhaeva, Yu.D. Tret'yakov, 2010, published in Rossiiskii Khimicheskii Zhurnal, 2010, Vol. 53, No. 2, pp. 56–67.

Nanocrystalline Ceria: Synthesis, Structure-Sensitive Properties, and Promising Applications

V. K. Ivanov[a], O. S. Polezhaeva[a], and Yu. D. Tret'yakov[b]

[a] *Kurnakov Institute of General and Inorganic Chemistry, Russian Academy of Sciences, Leninskii pr. 31, Moscow, 119991 Russia*
e-mail: van@igic.ras.ru

[b] *Lomonosov Moscow State University, Moscow, Russia*

Received January 10, 2009

Abstract—Directed search for further manifestations of size-dependent effects in the functional properties of nanomaterials constitutes a key line of nanotechnologies research. The major size-dependent effects were analyzed for nanocrystalline ceria. The practically significant techniques for preparation of ceria nanopowders with controllable micromorphology were analyzed. Selected promising applications of this material were described.

DOI: 10.1134/S1070363210030412

INTRODUCTION

Unusual functional properties of nanocrystalline ceria stem, above all, from the unique dependence of oxygen nonstoichiometry on the particle size in this compound. This feature, along with well-known changes in magnetic and optical properties with decreasing particle size [1, 2], can strongly exemplify size-dependent effects.

Here, we analyzed the practically significant techniques for preparation of ceria nanoparticles with controllable micromorphology. Also, we considered the major size-dependent effects characteristic for nano-crystalline ceria and described some promising, in particular, biomedical and energy-saving applications of this material.

Basic Techniques for Preparation of Nanocrystalline Ceria

Numerous techniques are currently available for preparation of micro- and nanosized ceria from solid, liquid, and gas phases. Traditionally, CeO_{2-x} is synthesized by solid-state reactions, in particular, via high-temperature thermolysis of cerium salts [3] and mechanochemical synthesis reactions, including those run at room temperature (see, e.g., [4, 5]). Gas-phase methods include vacuum evaporation of metallic cerium, followed by condensation of the metal particles in the cold zone and oxidation to CeO_{2-x} [6], as well as gas-phase thermolysis of volatile organic compounds of cerium (chemical deposition from the gas phase) [7]. The most extensively applied techniques are those based on liquid-phase synthesis of ceria in aqueous and nonaqueous media. This concerns, above all, direct precipitation of hydrated ceria from cerium(III) and cerium(IV) salts in strongly basic solutions (see, e.g., [8]), synthesis in microemulsions and reverse micelles formed by surfactants (e.g., sodium dioctylsulfosuccinate [9] or oleylamine [10]). The same group includes melt synthesis techniques.

The size of the resulting CeO_{2-x} nanoparticles typically ranges from 1–2 to 50 nm. Of special practical interest are techniques for synthesizing <5–10-nm particles, because size-dependent effects in ceria are predominantly observed specifically from this particle size range on. It should be noted that most of the above-mentioned techniques are either unsuitable for preparing nanoparticles with desired size or require expensive chemicals and equipment for their implementation.

Below, we consider techniques for synthesizing nanocrystalline ceria, as well as solid solutions and composites thereof, with controllable particle size and shape.

Preparation of Nanocrystalline Ceria by Homogeneous Precipitation

The solubility products of hydroxo compounds of cerium and ceria are very low, for which reason they are precipitated from cerium salt solutions under the action of bases in strongly oversaturated solutions. We found earlier [11, 12] that, like a number of other metal oxides, ceria is formed by the autocalytic mechanism, i.e., with autoacceleration. Often, this makes it nearly impossible to control the micromorphology of solid synthesis products. A good alternative can be found in the use of reactants that undergo slow hydrolysis with formation of hydroxide ions. This allows controlling the degree of oversaturation of the solutions and avoids local concentration gradients.

Synthesis of CeO_{2-x} in the Presence of Hexamethylenetetramine

Synthesis of metal oxides (in particular, ceria) by reacting hexamethylenetetramine with metal salt solutions can proceed in several stages. We found that the intermediates in CeO_{2-x} synthesis from aqueous solutions of cerium(III) salts and hexamethylenetetramine can include insoluble hydroxo compounds of cerium, in particular, cerium(III) hydroxocarbonate [13].

Hydrolysis of cerium salts in the presence of hexamethylenetetramine underlies numerous synthesis routes for nanocrystalline ceria [14–16]. Zhang et al. [15, 16] showed that the CeO_{2-x} nanoparticle size varies, nearly linearly, with the reaction time. The CeO_{2-x} particle growth dynamics is also governed by other factors, in particular, the reaction temperature and the molar ratio of reactants [13, 17]. By modifying the synthesis conditions it is possible to widely vary the size (from 10 to 50 nm) and shape of ceria nanoparticles [18]. In particular, a decrease in molar excess of hexamethylenetetramine over $Ce(NO_3)_3$ leads to extremely thin (<1-nm) CeO_{2-x} plates with oriented attachment (Fig. 1).

Homogeneous precipitation in the presence of hexamethylenetetramine is suitable for preparation of not only nanocrystalline ceria but also solid solutions thereof [19–21]. For example, Markmann et al. [19] synthesized praseodymium-doped ceria from aqueous solutions of cerium(III) nitrate and praseodymium chloride in the presence of hexamethylenetetramine at 100°C. The resulting nanoparticles are characterized by isotropic shape. With concentration of the initial cerium(III) nitrate solution increasing from 0.005 to 0.02 M the average particle size increases from 8.1 to 14.9 nm.

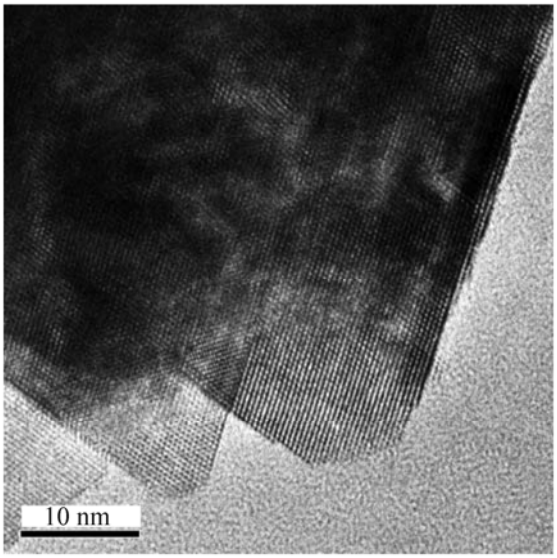

Fig. 1. Ceria nanoplates prepared from $Ce(NO_3)_3$/hexamethylenetetramine aqueous solutions (molar ratio 1:3) [18].

A similar technique was employed for preparing gadolinium- and samarium-doped ceria [21]. It was found that the Ce/Gd and Ce/Sm molar ratios in the resulting products correspond to the cation ratio in the initial solutions. Rare-earth ion doping of CeO_2 leads to more finely dispersed products.

Vasylkiv et al. [22, 23] proposed a modified technique for multistage synthesis of nanocrystalline oxide powders. It consists of the following stages: precipitation of metal oxide nanoparticles in the presence of hexamethylenetetramine; impregnation of oxide powders with colloid solutions of cyclotrimethylenetrinitramine; and heat treatment of the resulting nanocomposites under circumstances conducive to explosive decomposition of cyclotrimethylenetrinitramine. Combined, these stages produce negligibly aggregated nanoparticles which are promising candidates for preparation of CeO_{2-x}-based nanoceramics.

Synthesis of CeO_{2-x} in the Presence of Urea

Matijevic and Hsu [24] reported that, when heated in the presence of urea, cerium(III) salts are hydrolyzed into spindle- or rod-like particles of crystalline cerium(III) oxocarbonate $Ce_2O(CO_3)_2 \cdot H_2O$ or gel-like precipitates of the same composition. Those findings agree with the fact that, as established in [14], $Ce_2O(CO_3)_2 \cdot H_2O$ is the only product of $Ce(NO_3)_3$

hydrolysis in the presence of urea at 85°C, by contrast to the reaction with hexamethylenetetramine. At the same time, Hirano and Kato [25] showed that, under hydrothermal conditions (120–180°C), hydrolysis of cerium(III) salts in the presence of urea can yield two crystalline phases, orthorhombic cerium(III) oxocarbonate and hexagonal cerium(III) hydroxocarbonate $Ce(OH)CO_3$. The resultant products in each specific case will be determined by the choice of the initial cerium salt, the urea concentration, and the hydrothermal treatment temperature. Subsequent heat treatment (300–900°C) of the synthesized products yields nanocrystalline ceria with controllable particle size within 6–40 nm.

Hirano and Kato [26] used cerium(IV) sulfate and urea as precursors to directly synthesize nanocrystalline ceria under identical conditions. In that study, the difference in the products synthesized from Ce^{4+} and Ce^{3+} was attributed to the fact that the former is more prone to hydrolysis. The CeO_{2-x} particle size can be directly varied within 10–20 nm by varying the synthesis temperature and urea content in the reaction mixtures. The particles prepared by homogeneous precipitation are several times larger than those yielded by precipitation with aqueous ammonia, followed by hydrothermal treatment of the precipitates under identical conditions. This is most likely due to a lower effective concentration of the precipitating agent and the ensuing dominance of particle growth and smaller contribution from nucleation. In a similar manner, an increase in the urea concentration from 0.2 to 0.8 M causes the size of individual CeO_{2-x} crystallites to decrease by half, and that of the aggregates thereof, to double [27].

The shape and size of hydroxo compounds of cerium(III) and ceria prepared by hydrolysis in the presence of urea can be additionally controlled with the use of various templates (structure-forming agents). In particular, Wang et al. [28] introduced polyethylene glycols (molecular weight 1000 and 20000), as well as cetyl trimethylammonium bromide, into reaction mixtures. With various templates it is possible to prepare $Ce(OH)CO_3$ particles with shapes ranging from ellipse-like to octahedral, cross-like, etc. It was found that subsequent high-temperature annealing causes formation of CeO_{2-x} particles inheriting the $Ce(OH)CO_3$ particle shape. Zhang et al. [29] carried out hydrothermal treatment of reaction mixtures containing cerium nitrate, urea, and cetyl trimethylammonium bromide, followed by annealing of the solid reaction products at 500°C, and obtained thin rhombic CeO_{2-x} plates. Wu et al. [30] proposed a technique for preparation of CeO_{2-x} nanowires with the use of anodized porous alumina as template.

Homogeneous precipitation in the presence of urea is successfully applied for synthesizing CeO_{2-x}-based solid solutions and composites. Si et al. [31] prepared homogeneous $Ce_{1-x}Zr_xO_2$ solid solutions by hydrothermal treatment of ammonium-cerium(IV) nitrate, zirconyl nitrate, and urea solutions at 140°C, followed by annealing of the solid products at 500–900°C. Such solid solutions can also be synthesized directly by hydrothermal treatment of the reactants.

Cheng et al. [32] prepared samarium-doped nanocrystalline ceria by heating cerium(IV) sulfate, samarium nitrate, and urea solutions to 100°C. In those experiments, solid solutions were formed in several stages. These include coprecipitation of cerium and samarium hydroxides into primary particles substantially enriched in cerium and depleted in samarium relative to the stoichiometric composition; precipitation of the residual samarium in the hydroxide form onto the primary particle surface; and diffusion of the samarium ions deep inside the primary particles. Jobbagy et al. [33] suggested the use of homogeneous precipitation technique for preparing CeO_2/CuO nanocomposites, highly efficient in catalytic afterburning of carbon monoxide. This technique is also suitable for synthesizing other ceria-based nanocomposites.

Principal Relationships in Ceria Nanoparticle Growth under Hydrothermal Conditions

Hydrothermal treatment route belongs to those most extensively used for preparation of micro- and nanodisperse functional oxide materials with controllable micromorphology. The formation of metal oxides under hydrothermal conditions is generally a multistage process. The mechanism, kinetics, and temperature range for individual stages were reliably established for selected systems only.

Below, we present the data on ceria nanoparticle formation and growth in relation to the hydrothermal treatment conditions.

"Conventional" Hydrothermal Synthesis Route for Nanocrystalline Ceria

In the first experiments on hydrothermal synthesis of highly-dispersed powdered ceria the precursor was hydrated ceria $CeO_2 \cdot nH_2O$ precipitated by aqueous

ammonia from cerium(III) nitrate. Hydrothermal treatment of $CeO_2 \cdot nH_2O$ was carried out at 500, 600, and 700°C in distilled water, as well as in KF, LiCl, LiBr, K_2CO_3, $LiNO_3$, Li_2SO_4, and NaOH solutions. It was found that increases in treatment temperature and time, as well as introduction of mineralizing agents into the reaction mixture, caused the ceria particle to increase in size, on the whole. Depending on the synthesis conditions, the CeO_{2-x} particles ranged in size from 30 to 100 nm and over.

Hirano and Kato [35, 36] were the first to systematically examine how the temperature (120–200°C) and time (5–40 h) of hydrothermal treatment affect the ceria nanoparticle size. As reactants in those studies served hydrated CeO_{2-x} suspensions precipitated by aqueous ammonia from cerium(III) nitrate, cerium(IV) sulfate, and ammonium-cerium(IV) sulfate solutions. In hydrothermal treatment of the suspensions with the nitrate history at up to 180°C the size of the CeO_{2-x} crystallites was temperature-independent (~2 nm). With cerium(IV) sulfate as reactant, the particle size varied within 2.5–8.5 nm, depending on the treatment parameters (time, temperature) and suspension concentration.

Lakhwani and Rahaman [37] revealed parabolic kinetics for the CeO_{2-x} particle growth under hydrothermal conditions at 150–300°C and attributed this finding to Ostwald ripening (dissolution–crystallization). In hydrothermal treatment of ceria suspensions precipitated from $CeCl_3$ and $Ce(NO_3)_3$ solutions the particle growth dynamics for CeO_{2-x} with chloride and nitrate histories differ substantially. The particle size for CeO_{2-x} synthesized from $Ce(NO_3)_3$ varied within 9–20 nm, while that in the case of $CeCl_3$ remains virtually unchanged (13.5–15.5 nm). The factors responsible for this difference were not identified in [37]. These results are inconsistent with the dissolution–crystallization model employed in that study: The growth dynamics for nanoparticles in that case should be governed by their size solely and be independent of the history.

Wu et al. [38] examined the CeO_{2-x} particle growth dynamics under the hydrothermal conditions (18–240 h, 20–245°C) in relation to the acidity of the medium. In neutral and weakly alkaline media the ceria particles exhibited fairly slow growth, while in acid medium they rapidly increase in size. The degree of aggregation of CeO_{2-x} nanoparticles substantially decreased with decreasing pH of medium. The data reported in [38] agree, on the whole, with the results of a study by Tok et al. [39], in which hydrothermal treatment of hydrated ceria suspensions at 250°C for 6–24 h did no cause the CeO_{2-x} nanoparticles to significant increase in size (5–6 nm). That study revealed an increase in the CeO_{2-x} unit lattice parameter upon hydrothermal treatment, but the factors responsible for this phenomenon were not analyzed. By contrast, Malta et al. [40] reported that, in the course of hydrothermal treatment, the CeO_{2-x} unit cell parameter were unaffected both by the treatment temperature and time. Also, synthesis in open vessels (with reflux condenser) yielded more coarsely crystalline samples with larger oxygen nonstoichiometry compared to the samples prepared in autoclaves [40].

Microwave-Assisted Hydrothermal Synthesis of Nanocrystalline Ceria

Microwave-assisted synthesis of inorganic materials is gaining ever widening acceptance. This is due both to the unique features of this technique (in particular, rapid and uniform heating) and occurrence of nonthermal effects underlain by manyfold increase in the effective diffusion coefficients of ions [41, 42]. In a number of cases, microwave radiation is combined with other physical impacts on the reaction system, e.g., laser irradiation. Such combined synthesis methods include, in particular, microwave-assisted hydrothermal treatment.

There exist only fragmentary data on the preparation of nanocrystalline ceria under these conditions. In the first publication (of 2005) dedicated to microwave-assisted hydrothermal synthesis of CeO_{2-x}.

Yang et al. [43] described the procedure in which the reactants, ammonium–cerium(IV) nitrate and sodium hydroxide, were kept in a household microwave oven for 20 min. (This publication did not specify the size and other features of the synthesized nanoparticles.)

Bonamartini Corradi et al. [44] examined in detail the micromorphology of ceria nanopowders synthesized from analogous precursors in relation to the microwave-assisted hydrothermal synthesis conditions (reactant concentrations [Ce] = 0.1–2.5 M, [NaOH] = 1–10 M, treatment time 5–240 min). Variation of the synthesis parameters in the indicated ranges caused the particle size and specific surface area of the products to change from 4.0 to 5.8 nm and from 143 to 207 $m^2 g^{-1}$, respectively. Unfortunately, the characteristics of the synthesized samples were not compared to those of analogous samples prepared by conventional hydrothermal route. In this situation, one cannot judge

for certain whether or not there exist specific effects of microwave radiation on the reaction mixtures.

Gao et al. [45] carried out microwave-assisted hydrothermal synthesis of CeO_{2-x} at a fixed temperature (160°C) with different precipitating agents (NaOH, aqueous ammonia, urea, ethylene diamine, formamide) which were added to cerium salt solution before the treatment. In all cases the sole product was ceria with the particle size ranging from 2.6 to 8.6 nm. Slowly hydrolyzable chemicals (urea, ethylene diamine, formamide) led to larger CeO_{2-x} particles. It was found that the micromorphology is additionally affected by the concentration of the reactants. In particular, a decrease in the precipitating agent concentration leads to formation of larger particles. An increase in the synthesis time produces a similar effect. It was reported [45] that, under microwave heating, the synthesis time decreases several times, but the validity of this conclusion cannot be judged because of the lack of data on the technique applied for control tests.

Our data [18] suggest that the size of the CeO_{2-x} particles yielded by conventional and microwave-assisted hydrothermal treatments of freshly precipitated neutral suspensions of hydrated ceria is independent of the synthesis temperature and time. This suggests poor solubility of this compound in hydrothermal media. The narrowest particle size distribution was found in samples prepared by microwave-assisted hydrothermal synthesis at fairly high temperatures (180–210°C). The CeO_{2-x} nanopowders synthesized under those conditions are characterized by much smaller particle size and, correspondingly, by a larger specific surface area compared to samples prepared under similar conditions by conventional hydrothermal route. The difference in the micromorphology of the synthesized products is associated with the fact that microwave radiation affords uniform heat supply to the bulk of the reaction mixture and a much higher (nearly 15 times) heating rate. Thus, microwave radiation provides a fairly efficient additional control over CeO_{2-x} powder micromorphology.

Hydrothermal Synthesis of Unidimensional Ceria Nanostructures

Formation of anisotropic nanoparticles, in particular, in "mild chemistry" processes, is typical for substances with anisotropic crystal structure, e.g., ZnO and CdSe. As to substances with highly symmetrical (in particular, cubic) crystal structures, unidimensional (1D) nanostructures for them are typically synthesized with the use of surfactants or in porous solid matrices [46]. At the same time, a number of techniques were recently proposed for hydro- and solvothermal preparation of ceria nanorods, both with and without structure-forming agents. A feature common to all these techniques is that unidimensional CeO_{2-x} structures are synthesized in alkaline and strongly alkaline media. This, presumably, constitutes the critical precondition to formation of ceria nanorods.

The growth mechanism for 1D CeO_{2-x} nanostructures under hydro- and solvothermal conditions still remains to be convincingly established. There exist three basic models of ceria nanorod formation:

(1) topotactic inheritance of the structure of solid precursors;

(2) particle growth by the dissolution–crystallization mechanism (Ostwald ripening); and

(3) oriented attachment of isotropic crystallites with formation of anisotropic nanostructures.

A peculiar two-stage technique for synthesis of CeO_{2-x} nanorods with controllable particle size was proposed in [47–50]. Specifically, after precipitation at the chosen temperature (70 and 90°C) the resulting suspension are kept at a low temperature. The precipitate formed in the first minutes after mixing of the solutions is essentially a mixture of crystalline ceria and cerium(III) hydroxide phases; it consists predominantly of rod-shaped particles, which is typical for $Ce(OH)_3$. In the course of aging of the reaction mixture at 0°C the diffraction maxima characteristic for $Ce(OH)_3$ disappear only at the synthesis time as long as 20 h. As shown by transmission electron microscopic examination, the resulting CeO_{2-x} particles were also shaped as rods 8–10 nm in diameter with length of over 200 nm; they are comprised of a multitude of smaller particles. On this basis it was suggested that CeO_{2-x} nanorods topotactically inherit the shape of the initial $Ce(OH)_3$ nanorods.

The hypothesized formation of 1D CeO_{2-x} nanostructures via precursor structure inheritance was supported by Zhou et al. [51]. In that study, $Ce(OH)_3$ nanorods of several hundreds of nanometers in length with the diameter of 15–25 nm were synthesized by hydrothermal treatment of suspensions prepared by mixing aqueous solutions of $Ce_2(SO_4)_3$ and NaOH. Air exposure of the samples led to gradual oxidation of $Ce(OH)_3$ to CeO_{2-x}, with the product preserving the

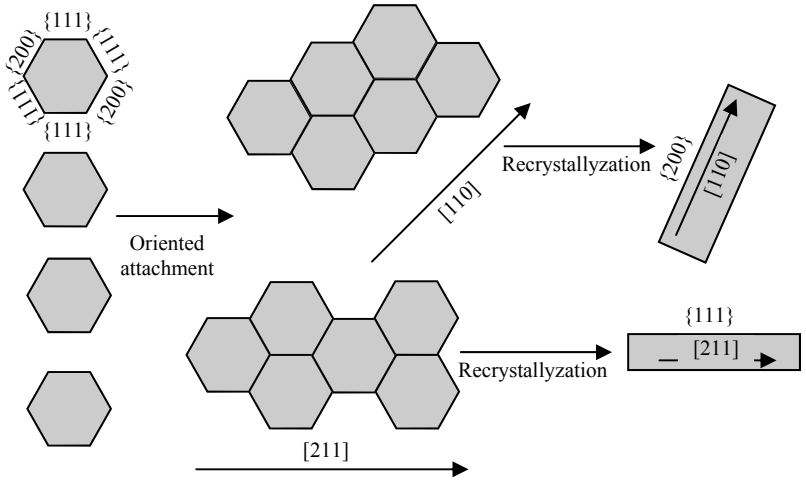

Fig. 2. Hypothesized scheme of ceria nanorod formation by oriented attachment of isotropic crystallites, followed by Ostwald ripening [60].

nanorod shape. Also, a peculiar technique was proposed for preparation of CeO_{2-x} nanotubes via treating partially oxidized $Ce(OH)_3$ nanorods with hydrogen peroxide [51].

Thus, it was shown experimentally [47–52] that the microstructure inheritance may be a key (though, probably, not the unique) factor governing the shape of CeO_{2-x} nanoparticles.

At the same time, there is a need in much better substantiation of the hypothesized formation of 1D CeO_{2-x} nanostructures via CeO_{2-x} particle growth by the dissolution–crystallization mechanism exclusively. For example, Yang et al. [53] believes that formation of particles with various shapes and sizes (nanorods at moderate temperatures and isotropic particles at higher temperatures) is decided by the temperature dependence of the solubility of CeO_{2-x}: At fairly low synthesis temperatures the dissolved ceria concentration will be low and the particles will grow along selected crystallographic axes solely. An alternative viewpoint [54, 55] assigns the deciding role in formation of anisotropic CeO_{2-x} particles by the dissolution–crystallization mechanism to the anions that are sorbed on the nanoparticle surface and thereby preclude growth along certain crystallographic axes.

An alternative mechanism of 1D ceria nanostructure formation is oriented attachment [56–58]. Specifically, two primary particles collide and coalesce in a liquid medium with the same crystallographic orientation. This is followed by coherent intergrowth of the nanoparticles into single-crystalline particles or polycrystals separated by twin boundaries or other planar defects.

Si et al. [59] found that coalescence of colloid ceria particles prepared by treating a mixture of ethanolic solutions of cerium(III) nitrate and alkyl amines (or potassium hydroxide) under hydrothermal conditions (180°C, 24 h) can lead to mutual attachment with formation of chain aggregates. Introduction of polyvinylpyrrolidone into the reaction mixture causes noticeable enhancement of orientation of the particles, and individual particles are intergrown into single-crystalline nanowires.

The first experimental validation of oriented attachment in the absence of structure-forming agents was provided by Du et al. [60]. It was shown that hydrothermal treatment of suspensions prepared by mixing aqueous solutions of $Ce(NO_3)_3$ and NaOH heated to boiling leads to single-crystalline ceria nanorods growing along the [211] and [110] axes. As demonstrated by a series of additional experiments, the intermediate stage in nanorod formation consists in oriented intergrowth of isotropic CeO_{2-x} nanoparticles. The resulting irregularly-shaped aggregates undergo recrystallization during subsequent hydrothermal treatment. A hypothesized process scheme is shown in Fig. 2.

We found [18] that the content of nanorods is at a maximum at not very high temperatures (up to 120°C) and brief synthesis times. Formation of nanorods is

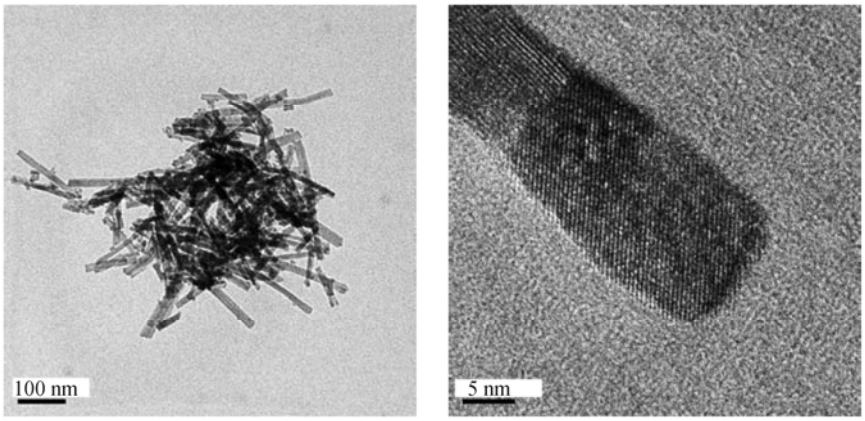

Fig. 3. Electron images of CeO_{2-x} nanorods prepared by hydrothermal treatment in alkaline media [18].

also promoted by increase in alkali concentration in the reaction mixture (Fig. 3). Taken together, our results suggest that these are compound CeO_{2-x} nanorods formed by a mixed mechanism involving dissolution–crystallization and oriented attachment of CeO_{2-x} particles.

Oxygen Nonstoichiometry of Nanodispersed Ceria

For many substances (e.g., gold [61]) the unit cell parameters tend to decrease with crystallite size reduction to nanoscales. At the same time, certain oxide compounds (including CeO_{2-x}) exhibit the opposite trend: The unit cell parameter tends to increase with decreasing particle size. This trend was for the first time revealed by Tsunekawa et al. [62] for CeO_{2-x} particles stabilized by anionic surfactants [63]. The observed increase in the unit cell parameter from 0.545 to 0.556 nm with particle size decreasing from 6.7 to 2.1 nm was associated with partial removal of oxygen atoms in the surface layer from certain crystallographic sites. This leads to oxygen vacancies, in parallel with decrease in the apparent oxidation state of cerium. Model calculations predicted the critical size of 1.5 nm for the CeO_{2-x} particles in the case of exhaustive conversion of Ce^{4+} to Ce^{3+}.

More recent studies [19, 64, 65] confirmed an increase in the unit cell parameter with decreasing CeO_{2-x} particle size. An electron energy loss spectroscopic examination by Wu et al. [64] revealed a stronger oxygen nonstoichiometry for the nanoparticle surface compared to the bulk, with the surface composition being close to Ce_2O_3. The nonstoichiometric surface layer thickness tends to drastically increase with decreasing particle size. It that study, the apparent oxidation state of cerium was estimated at +3 already for particles measuring 3 nm in diameter, which is twice the value of 1.5 nm obtained in [62].

The crystal cell parameters for CeO_{2-x} nanoparticles of different sizes, reported by different researchers, are inconsistent. Tsunekawa et al. [66, 67] attributed this fact to different shapes of the CeO_{2-x} nanoparticles: Steeper curves are observed for particles characterized by negligible faceting [62, 64], and smoother curves, for octahedral particles [19]. However, a limited spectrum of the studied CeO_{2-x} samples prevents identification of factors that are really responsible for these differences.

A correlation between the oxygen nonstoichiometry and nanocrystalline ceria particle size was validated by Raman spectroscopic examinations [68–73] in which the Raman mode at 464 cm^{-1} corresponding to symmetric Ce–O^8 vibrations proved to be extremely sensitive to size-dependent changes in oxygen nonstoichiometry. A decrease in the CeO_{2-x} particle size causes systematic changes in the Raman spectra. A shift of the Raman peak to lower energies is associated with an increase in the crystal cell parameter of ceria, and the peak broadening, with inhomogeneous lattice strains.

The X-ray photoelectron spectroscopic examination of the oxygen nonstoichiometry for CeO_{2-x} nanoparticles of different sizes [74] provides plain evidence to an increase in the relative content of Ce^{3+} with decreasing CeO_{2-x} particle size. It should be noted, however, that this technique overestimates Ce^{3+} content in micro- and nanocrystalline CeO_{2-x} samples even at minimal analysis times [75], and the Ce^{3+} content in the samples of interest can vary not only

with size but also with preparation conditions for the particles [76, 77].

Changes in the oxygen nonstoichiometry of CeO_{2-x} directly affect the electronic properties of ceria which, for this reason, acquires the properties of a wide-band gap semiconductor. Examinations of colloid solutions of ceria nanoparticles [78–80] showed that, with decreasing particle size, the forbidden band width naturally tends to increase for both direct and indirect transitions. Zhang et al. [15] suggested the use of UV-visible spectroscopy for controlling the growth of CeO_{2-x} particles immediately during their synthesis from cerium salt solutions. Our data [13, 17, 81] suggest that the indicated technique is actually efficient in examining the growth dynamics for CeO_{2-x} particles synthesized by rapid and homogeneous hydrolysis routes. At the same time, the forbidden band width for CeO_{2-x} nanoparticles can be determined not only by their size but also by their preparation conditions which additionally affect the oxygen nonstoichiometry of ceria [82].

Promising Applications of Nanocrystalline Ceria

UV Radiation Filters

State of the art UV radiation filters employ for the most part titania or zinc oxide as active components. The latter are able of efficiently dissipating the UV radiation energy without formation of singlet oxygen and other reactive species [83]. At the same time, numerous studies revealed extremely high photocatalytic activity of nanodispersed powders of these compounds [84, 85]. Also, *in vitro* and *in vivo* experiments [83, 86] showed that titania destroys photocatalytically not only organic components of sunscreen creams but also the DNA molecules. Wamer et al. [87] revealed photocytotoxicity of titania towards skin fibroblasts. This casts reasonable doubts in the efficiency of existing UV filters [83].

The main component of UV radiation filters can be found in ceria-based nanocrystalline materials [88–90]. They are advantageous in terms of efficient absorption of UV radiation, transparency in the visible, and a yellow-brown color, which is close to that of skin. However, noticeable catalytic activity of CeO_{2-x} in organics oxidation can prevent its application in sunscreen compositions. For this reason it is recommended that ceria-based solid solutions, in particular, $Ce_{1-x}Zn_xO_{2-x}$ and $Ce_{1-x}Ca_xO_{2-x}$, rather than individual ceria be used for these purposes. Leaving virtually unaffected the optical characteristics of materials, such doping significantly decreases their catalytic activity (as demonstrated in the case of castor oil oxidation).

Tabe and Sato [91] carried out a comparative study of the catalytic activities exhibited by samples of nanocrystalline ceria doped with Mg^{2+}, Ca^{2+}, Sr^{2+}, Ba^{2+}, Zn^{2+},Y^{3+}, La^{3+}, Nd^{3+}, Sm^{3+}, Eu^{3+}, and Tb^{3+} in castor oil oxidation, as well as of the photocatalytic activities in phenol decomposition. The suppression of catalytic and photocatalytic activities was most profound in the case of calcium- and zinc-doped CeO_{2-x}, in which the average size of cerium particles was significantly decreased (to 2–4 nm).

The catalytic activity of $Ce_{1-x}M_xO_{2-x}$ nanoparticles can be further suppressed by deposition onto their surface of amorphous silica via hydrolysis of sodium silicate or tetraethoxysilane [92–95]. Those data were further validated by comparative examination of the chemiluminescence intensities of CeO_{2-x}-based nanocomposites under UV irradiation exposure [92, 95].

Thus, ceria-based nanomaterials may be regarded as suitable candidates for application in the new generation of inorganic UV filters. However, their applicability can be finally judged after thorough biocompatibility testing only.

Biological Applications of Ceria

A long history of medicinal application of cerium compounds dates back to the first relevant publications of 1950s. The active component for the overwhelming majority of medicinal agents was found in water-soluble cerium(III) salts, as well as in some insoluble compounds, e.g., cerium stearate and cerium oxalate, in particular, as colloid solutions [96].

The mechanism by which cerium(III) compounds affect human body still remains to be elucidated more clearly. Jakupec et al. [96] associated the biological activity exhibited by cerium salts in some cases with close ionic radii of Ce^{3+} and Ca^{2+}, for which reason cerium ions can partially substitute calcium ions in some biomolecules. This can be responsible, e.g., for anticoagulation action of cerium and other lanthanide compounds. Also, it is well known that cerium(III) salts are suitable as antiemetics, bacteriostatics, and bactericides, as well as immunomodulators and anti-tumor preparations [96].

At the present time, there are no systematic data on the biological activity of nanodispersed ceria. Never-

theless, individual publications attest to much promise held by CeO_{2-x} for biomedical applications.

Schubert et al. [97] and Das et al. [98] examined the neuroprotective action of nanodispersed CeO_{2-x}. In experimental studies of the protective effect of CeO_{2-x} under oxidative stress, a suspension of CeO_{2-x} nanoparticles in a growth medium was added to HT22 line neurons. Subsequently, the cells were exposed to glutamic acid which causes cell destruction by the oxytosis mechanism. It was found that the CeO_{2-x} nanoparticles prevent, to a significant extent, cell destruction. The amount of the cells that survived is dependent on the CeO_{2-x} content and independent of the nanoparticle size. As to protective action mechanism, it was found [97] that CeO_{2-x} nanoparticles can directly bind the reactive oxygen-containing compounds, which fact was attributed to the oxygen nonstoichiometry of nanocrystalline ceria.

Examinations of how ceria nanoparticles (3–5 nm) affect the survival of spinal cord neurons [98] showed that CeO_{2-x} significantly decelerates dying of cells in the populations. The reason is a prominent ability of CeO_{2-x} for free radical binding. It was presumed that, when combined with other antioxidants, ceria can mitigate the consequences of spinal cord injuries.

Chen et al. [99] provided *in vitro* and *in vivo* validation of antioxidant activity of nanocrystalline ceria. In that study, introduction of CeO_{2-x} into rat retina substantially prevented dying of photoreceptor cells under subsequent intense light radiation exposure. Electroretinographic examinations showed that the retina functions also remained virtually intact. When CeO_{2-x} is introduced into the vitreous body after irradiation, the survival of photoreceptor cells also increases. The reactive oxygen-containing compounds were directly bound by CeO_{2-x} nanoparticles. Hence, the latter hold promise for prevention and treatment of Alzheimer's, Parkinson's, and Huntington's diseases.

Rzigalinski [100] reported on ability of CeO_{2-x} nanoparticles for significantly enhancing the viability of brain cells, in particular, astrocytes, neurons, microglyal cells, and oligodendrocytes. In the presence of nanodispersed ceria those cell cultures preserve their morphological and biochemical characteristics for 6–8 months against 26–30 days under ordinary conditions. Such effect cannot be achieved with microcrystalline ceria, as well as with nanocrystalline powdered oxides of other metals (including Pr, La, Ti, Ru).

Of special practical significance is prophylactic application of CeO_{2-x} in radiotherapy cancer treatment (ceria causes the amount of killed healthy cells to decrease by 40–70%). The CeO_{2-x} nanoparticles can cause an increase in the life span of not only microbut also macroorganisms [100]. In particular, they caused increases in the median and maximal life spans in Drozophilas. This phenomenon is also underlain by antioxidant action of ceria nanoparticles.

We examined the effect exerted by nanocrystalline ceria on TG1 genetically engineered *Escherichia coli* strain whose bioluminescence intensity correlates with the enzymatic activity of the bacteria. Our tests showed that, up to the maximal concentration (20000 mg l^{-1}), CeO_{2-x} in an aqueous suspension was not toxic toward the test culture. We demonstrated for the first time that, with decreasing CeO_{2-x} particle size, the bioactivity of the powders tends to significantly increase [101]. The correlation between the particle size and bioactivity of CeO_{2-x} nanopowder can be explained by increases in the bulk and surface nonstoichiometries with decreasing CeO_{2-x} nanoparticle size.

Electrochromic Devices

The last decade has witnessed significant progress in development of electrochromic coatings and devices thereof. The operation of the latter is underlain by the concept that, upon passing an electric current therethrough, positive ions (typically Li^+) diffuse from the counter-electrode to the electrochromic layer, thereby affecting its transparency. The practical application of electrochromic coatings is constrained by moderate performance characteristics of counter-electrodes. Indeed, the development of efficient electrochromic materials can be treated as a problem that has been solved in general (with tungsten trioxide as the most promising material). At the same time, the task of development of counter-electrode materials is far from being accomplished. In particular, this concerns the color changes induced by lithium intercalation/deintercalation in nickel and cobalt oxides employed in these materials.

Boudry et al. [102] suggested CeO_{2-x} as a candidate material for counter-electrodes. Its major advantages include the reversible Li^+ intercalation/deintercalation and invariance of the optical characteristics under exploitation, as well as the lack of absorption in the visible, the UV radiation blocking ability (this is of special significance for electrochromic polymers), and,

lastly, not very high cost. The drawback suffered by CeO_{2-x} in counter-electrode applications is associated with not very high rate of lithium ion intercalation into ceria.

In this context, it was suggested that ceria- and titania-based (1:1) nanocomposites be used as counter-electrode materials [102]. They afford a tenfold increase in the effective diffusion coefficient for lithium and the corresponding decrease in the response time of the electrochromic coating.

Keomany et al. [103, 104] examined the functional characteristics of $(CeO_2)_x$–$(TiO_2)_{1-x}$ thin films synthesized by the sol-gel route. Each of the films is essentially an amorphous TiO_2 matrix with nanocrystalline CeO_{2-x} (1–5 nm) inclusions. Those studies showed that, in changing from neat CeO_{2-x} to $(CeO_2)_{0.25}$–$(TiO_2)_{0.75}$, the effective diffusion coefficient of Li^+ tends to increase from 1.5×10^{-14} to 1×10^{-12} $cm^2\ s^{-1}$. However, films with low cerium content exhibit too low capacities with respect to lithium ions. Verma et al. [105] took cerium(III) chloride and $Ti(OC_3H_7)_4$ as precursors for preparing $(CeO_2)_x$–$(TiO_2)_{1-x}$ films. As shown by X-ray phase analysis, crystalline ceria is formed in films at high cerium content (>66%) only, with CeO_{2-x} crystallites measuring up to 14 nm in size. The structure of the resulting films is fairly coarse-grained, but the current densities for them exceed by nearly an order of magnitude those reported in [104]. Hence, the functional properties of the films substantially depend on the specific precursors and synthesis conditions. The optimal electrochemical and optical characteristics are exhibited by films containing 50% cerium.

Naturally, a much better quality of the CeO_2–TiO_2 composites compared to individual nanocrystalline ceria stimulated the interest in development of new composite materials on the CeO_{2-x} basis. A CeO_2–SnO_2 (17% SnO_2) composite synthesized in [106] exhibited a high capacity with respect to lithium ions and a brief response time. However, Huggins [107] showed that lithium intercalation can lead to partial reduction of tin dioxide to SnO and Sn. This casts doubts in suitability of CeO_2—SnO_2 composites as counter-electrode materials for electrochromic applications.

Berton et al. [108] and Zhu et al. [109] examined the microstructure, as well as the optical and electrochemical characteristics of CeO_2–SiO_2 films. It was found that, when the SiO_2 content increases from 0 to 35%, the ceria particles tend to decrease in size from 7 to 3 nm, with the charge density increasing up to a maximum achieved at 35% Si. A cyclic voltammetry examination showed that lithium intercalation/deintercalation into thin CeO_2–SiO_2 films is totally reversible even after 2000 cycles, but the capacity with respect to lithium is decreased by 40%.

It was suggested [110–112] that CeO_2–ZrO_2 solid solutions be used as counter-electrode materials. In that case, the effective diffusion coefficients for lithium can reach 1×10^{-12} $cm^2\ s^{-1}$, which is comparable with the data for CeO_2–TiO_2 nanocomposites [104]. The functional characteristics of the resulting materials fully satisfy the requirements posed on counter-electrodes in electrochromic devices.

Solar Cells

Ceria is part of antireflective coatings applied in silicon solar cells [113], which is primarily due to its high refractive index estimated at 2.4–2.56 for thin CeO_{2-x} films against 2.23–2.33 for the bulk material [114]. Also, the unit cell parameters of ceria and silica are very close, which allows preparing high-quality epitaxial films thereof [115].

Ceria is not a classical semiconductor, which typically prevents it from being treated as a photoactive material. However, data by Corma et al. [116] suggest the opposite: Mesoporous ceria films comprised of crystallites 5 nm in diameter are suitable as working components of solar cells. In particular, by contrast to coarsely-dispersed ceria, those materials are characterized by prolonged lifetime of photoinduced charge carriers, which exceeds that for nanocrystalline titania (Degussa P-25). Zirconium and lanthanum doping of CeO_{2-x} allows varying the forbidden band width [116]. This offers prospects for development of visible radiation-sensitive solar cells operating without photosensitizers.

Lira-Cantu and Krebs [117] developed hybrid polymeric solar cells based on nanodispersed CeO_{2-x} and CeO_2–TiO_2 with poly[2-methoxy-5-(2'-ethylhexyloxy)-1,4-phenylene vinylene].

As validated by relevant studies, ceria is suitable in principle for solar cell applications. However, the current strength generated by such cells is 2–3 times lower than that achieved with titania. The advantages offered by CeO_{2-x}-based cells include more stable characteristics and longer (threefold increased) service life compared to TiO_2-based devices.

CONCLUSIONS

Nanocrystalline ceria is a unique polyfunctional material having a broad spectrum of applications owing to unusual physicochemical properties. These include, in particular, a pronounced size dependence of such essential characteristics as oxygen nonstoichiometry and optical and electrophysical properties. In this context, an item of special urgency is to develop highly efficient scalable technologies for preparation of nanodispersed CeO_{2-x} powders with preset micromorphology and controllable particle size distribution to be suitable as precursors for preparation of functional nanomaterials and nanocomposites.

Of no less significance are studies of the physicochemical properties of nanocrystalline CeO_{2-x} and certification of nanomaterials thereof. In this context, the key role will be undoubtedly played by techniques utilizing state of the art neutron and synchrotron radiation sources. Lastly, special attention is to be paid to development and clinical trials of bioactive preparations containing ceria nanoparticles.

The applications of nanocrystalline ceria are by no means exhausted by the above-described examples. Ceria is part of numerous catalysts, protective corrosion-resistant coatings for metals and alloys, polishing mixtures, and abrasives (in particular, those intended for chemicomechanical treatment of silicon wafer surface in micro- and nanoelectronics), sensors, biosensors, etc. Development and improvement of the functional characteristics of these and other CeO_{2-x}-based nanomaterials require interdisciplinary efforts by experts in chemistry, physics, materials science, biology, and medicine.

ACKNOWLEDGMENTS

This review.study was financially supported by the Russian Foundation for Basic Research (project no. 08-03-00471), "Development of Scientific Principles of New Chemical Technologies with Preparation of Experimental Batches of Substances and Materials" Program of the Chemistry and Materials Science Division, Russian Academy of Sciences, and "Development of Methods for Synthesis of Chemical Substances and Preparation of New Materials" Program of the Presidium of the Russian Academy of Sciences.

REFERENCES

1. Cao, G., *Nanostructures and Nanomaterials: Synthesis, Properties, and Applications*, London: Imperial College Press, 2004.
2. Rao, C.N.R., Thomas, P.J., and Kulkarni, G.U., *Nanocrystals: Synthesis, Properties, and Applications*, Berlin: Springer, 2007.
3. Adachi, G. and Imanaka, N., *Chem. Rev*., 1998, vol. 98, pp. 1479–1514.
4. Li, F., Yu, X., Pan, H., Wang, M., and Xin, X., *Solid State Sci*., 2000, vol. 2, pp. 767–772.
5. Yu, X., Li, F., Ye, X., Xin, X., and Xue, Z., *J. Am. Ceram. Soc*., 2000, vol. 83, pp. 964–966.
6. Tschöpe, A. and Ying, J.Y., *Nanostr. Mater*., 1994, vol. 4, pp. 617–619.
7. Bui, W., Choy, K.L., Stelzer, N.H.J., and Scoonman, J., *Solid State Ionics*, 1999, vol. 116, pp. 225–228.
8. Imoto, F., Nanataki, F., and Kaneko, S., *Ceram. Trans*., 1988, vol. 1, pp. 204–210.
9. Bumajdad, A., Zaki, M.I., Eastoe, J., and Pasupulety, L., *Langmuir*, 2004, vol. 20, pp. 11223–11233.
10. Liu, Y.L., He, S.T., Uehara, M., and Maeda, H., *Chem. Lett*., 2007, vol. 36, pp. 764–765.
11. Ivanov, V.K., Sharikov, F.Yu., Polezhaeva, O.S., and Tret'yakov, Yu.D., *Dokl. Ross. Akad. Nauk, Ser. Khim*., 2006, vol. 411, no. 4, pp. 485–487.
12. Sharikov, F.Yu., Ivanov, V.K., Sharikov, Yu.V., and Tret'yakov, Yu.D., *Zh. Neorg. Khim*., 2006, vol. 51, no. 12, pp. 1957–1962.
13. Polezhaeva, O.S., Yaroshinskaya, N.V., and Ivanov, V.K., *Neorg. Mater*., 2008, vol. 44, no. 1, pp. 57–63.
14. Chen, P.-L. and Chen, I.-W., *J. Am. Ceram. Soc*., 1993, vol. 76, pp. 1577–1583.
15. Zhang, F., Jin, Q., and Chan, S.-W., *J. Appl. Phys*., 2004, vol. 95, pp. 4319–4326.
16. Zhang, F., Chan, S.-W., Spanier, J.E., Apak, E., Jin, Q., Robinson, R.D., and Herman, I.P., *Appl. Phys. Lett*., 2002, vol. 80, pp. 127–129.
17. Polezhaeva, O.S., Yaroshinskaya, N.V., and Ivanov, V.K., *Zh. Neorg. Khim*., 2007, vol. 52, no. 8, pp. 1266–1271.
18. Polezhaeva, O.S., *Cand. Sci. (Chem.) Dissertation*, Moscow: Inst. Obshch. Neorg. Khim. Ross. Akad. Nauk, 2008.
19. Markmann, J., Tschöpe, A., and Birringer, R., *Acta Mater*., 2000, vol. 50, pp. 1433–1440.
20. Rojas, T.C. and Ocana, M., *Scr. Mater*., 2002, vol. 46, pp. 655–660.
21. Li, J.-G., Wang, Y., Ikegami, T., Mori, T., and Ishigaki, T., *Mater. Sci. Eng. B*, 2005, vol. 121, pp. 54–59.
22. Vasylkiv, O., Sakka, Y., and Skorokhod, V.V., *J. Am. Ceram. Soc*., 2006, vol. 89, pp. 1822–1826.

23. Vasylkiv, O., Sakka, Y., and Skorokhod, V.V., *J. Eur. Ceram. Soc*., 2007, vol. 27, pp. 585–592.
24. Matijevic, E. and Hsu, W.P., *J. Coll. Int. Sci*., 1987, vol. 118, pp. 506–522.
25. Hirano, M. and Kato, E., *J. Mater. Sci. Lett*., 1999, vol. 18, pp. 403–405.
26. Hirano, M. and Kato, E., *J. Am. Ceram. Soc*., 1999, vol. 82, pp. 786–788.
27. Hirano, M. and Inagaki, M., *J. Mater. Chem*., 2000, vol. 10, pp. 473–477.
28. Wang, S., Gu, F., Li, C., and Cao, H., *J. Cryst. Growth*, 2007, vol. 307, pp. 386–394.
29. Zhang, D., Huang, L., Zhang, J., and Shi, L., *J. Mater. Sci.,* 2008, vol. 43, pp. 5647–5650.
30. Wu, G.S., Xie, T., Yuan, X.Y., Cheng, B.C., and Zhang, L.D., *Mater. Res. Bull*., 2004, vol. 39, pp. 1023–1028.
31. Si, R., Zhang, Y.-W., Li, S.-J., Lin, B.-X., and Yan, C.-H., *J. Phys. Chem. B*, 2004, vol. 108, pp. 12481–12488.
32. Cheng, M.-Y., Hwang, D.-H., Sheu, H.-S., and Hwang, B.-J., *J. Power Sources*, 2008, vol. 175, pp. 137–144.
33. Jobbagy, M., Marino, F., Schonbrod, B., Baronetti, G., and Laborde, M., *Chem. Mater*., 2006, vol. 18, pp. 1945–1950.
34. Tani, E., Yoshimura, M., and Somiya, S., *J. Mater. Sci. Lett*., 1982, vol. 1, pp. 461–462.
35. Hirano, M. and Kato, E., *J. Am. Ceram. Soc*., 1996, vol. 79, pp. 777–780.
36. Hirano, M. and Kato, E., *J. Mater. Sci. Lett*., 1996, vol. 15, pp. 1249–1250.
37. Lakhwani, S. and Rahaman, M.N., *J. Mater. Res*., 1999, vol. 14, pp. 1455–1461.
38. Wu, N.-C., Shi, E.-W., Zheng, Y.-Q., and Li, W.-J., *J. Am. Ceram. Soc*., 2002, vol. 85, pp. 2462–2468.
39. Tok, A.I.Y., Boey, F.Y.C., Dong, Z., and Sun, X.L., *J. Mater. Proc. Tech*., 2007, vol. 190, pp. 217–222.
40. Malta, L.F.B., Caffarena, V.R., Medeiros, M.E., and Ogasawara, T., *J. Therm. Anal. Calor*., 2004, vol. 75, pp. 901–910.
41. *Microwave-Enhanced Chemistry*, Kingston, H.M. and Haswell, S.J., Eds., Washington: ACS, 1997.
42. Vanetsev, A.S. and Tret'yakov, Yu.D., Usp. Khim., 2007, vol. 76, pp. 435–453.
43. Yang, H., Huang, C., Tang, A., Zhang, X., and Yang, W., *Mater. Res. Bull*., 2005, vol. 40, pp. 1690–1695.
44. Bonamartini Corradi, A., Bondioli, F., Ferrari, A.M., and Manfredini, T., *Mater. Res. Bull*., 2006, vol. 41, pp. 38–44.
45. Gao, F., Lu, Q., and Komarneni, S., *J. Nanosci. Nanotechnol*., 2006, vol. 6, pp. 3812–3819.
46. Wu, G.S., Xie, T., Yuan, X.Y., Cheng, B.C., and Zhan, L.D., *Mater. Res. Bull*., 2004, vol. 39, pp. 1023–1028.
47. Chen, H.-I. and Chang, H.-Y., *Solid State Comm*., 2005, vol. 133, pp. 593–598.
48. Chen, H.-I. and Chang, H.-Y., *Ceram. Int*., 2005, vol. 31, pp. 795–802.
49. Chang, H.-Y. and Chen, H.-I., *J. Cryst. Growth*, 2005, vol. 283, pp. 457–468.
50. Han, W.-Q., Wu, L., and Zhu, Y., *J. Am. Chem. Soc*., 2005, vol. 127, pp. 12814–12815.
51. Zhou, K., Yang, Z., and Yang, S., *Chem. Mater*., 2007, vol. 19, pp. 1215–1217.
52. Mai, H.-X., Sun, L.-D., Zhang, Y.-W., Si, R., Feng, W., Zhang, H.-P., Liu, H.-C., and Yan, C.-H., *J. Phys. Chem. B*, 2005, vol. 109, pp. 24380–24385.
53. Yang, Z., Zhou, K., Liu, X., Tian, Q., Lu, D., and Yang, S., *Nanotechnology*, 2007, vol. 18, pp. 185606-1–185606-4.
54. Higashine, Y. and Fujihara, S., *J. Ceram. Soc. Jpn*., 2007, vol. 115, pp. 916–919.
55. Huang, P.X., Wu, F., Zhu, B.L., Gao, X.P., Zhu, H.Y., Yan, T.Y., Huang, W.P., Wu, S.H., and Song, D.Y., *J. Phys. Chem. B*, 2005, vol. 109, pp. 19169–19174.
56. Penn, R.L. and Banfield, J.F., *Geochim. Cosmochim. Acta*, 1999, vol. 63, pp. 1549–1557.
57. Penn, R.L. and Banfield, J.F., *Am. Mineral*., 1998, vol. 83, pp. 1077–1082.
58. Penn, R.L. and Banfield, J.F., *Science*, 1998, vol. 281, pp. 969–971.
59. Si, R., Zhang, Y.-W., You, L.-P., and Yan, C.-H., *J. Phys. Chem. B*, 2006, vol. 110, pp. 5994–6000.
60. Du, N., Zhang, H., Chen, B., Ma, X., and Yang, D., *J. Phys. Chem. C*, 2007, vol. 111, pp. 12677–12680.
61. Mays, C.W., Vermaak, J.S., and Kuhlmann-Wilsdorf, D., *Surf. Sci*., 1968, vol. 12, pp. 134–140.
62. Tsunekawa, S., Sivamohan, R., Ito, S., Kasuya, A., and Fukuda, T., *Nanostruct. Mater*., 1999, vol. 11, pp. 141–147.
63. Tsunekawa, S., Sivamohan, R., Ohsuga, T., Kasuya, A., Takahashi, H., and Tohji, K., *Mater. Sci. Forum*, 1999, vols. 315–317, pp. 439–445.
64. Wu, L.J., Wiesmann, H.J., Moodenbaugh, A.R., Klie, R.F., Zhu, Y.M., Welch, D.O., and Suenaga, M., *Phys. Rev. B*, 2004, vol. 69, pp. 125415-1–125415-9.
65. Deshpande, S., Patil, S., Kuchibhatla, S.V.N.T., and Seal, S., *Appl. Phys. Lett*., 2005, vol. 87, pp. 133113-1–133113-3.
66. Tsunekawa, S., Ito, S., and Kawazoe, Y., *Appl. Phys. Lett*., 2004, vol. 85, pp. 3845–3847.
67. Tsunekawa, S., Wang, J.-T., and Kawazoe,Y., *J. Alloys Comp*., 2006, vols. 408–412, pp. 1145–1148.
68. Graham, G.W., Weber, W.H., Peters, C.R., and Usmen, R., *J. Catal*., 1991, vol. 130, pp. 310–313.

69. Weber, W.H., Hass, K.C., and McBride, J.R., *Phys. Rev. B,* 1993, vol. 48, pp. 178–185.
70. Kosacki, I., Suzuki, T., Anderson, H.U., and Colomban, P., *Solid State Ionics*, 2002, vol. 149, pp. 99–105.
71. Kosacki, I., Petrovsky, V., and Anderson, H.U., *J. Am. Ceram. Soc*., 2002, vol. 85, pp. 2646–2650.
72. McBride, J.R., Hass, K.C., Poindexter, B.D., and Weber, W.H., *J. Appl. Phys*., 1994, vol. 76, pp. 2435–2441.
73. Spanier, J.E., Robinson, R.D., Zhang, F., Chan, S.-W., and Herman, I.P., *Phys. Rev. B*, 2001, vol. 64, pp. 245407-1–245407-8.
74. Tsunekawa, S., Fukuda, T., and Kasuya, A., *Surf. Sci*., 2000, vol. 457, pp. L437–L440.
75. Zhang, F., Wang, P., Koberstein, J., Khalid, S., and Chan, S.-W., *Surf. Sci*., 2004, vol. 563, pp. 72–82.
76. Natile, M.M., Boccaletti, G., and Glisenti, A., *Chem. Mater*., 2005, vol. 17, pp. 6272–6286.
77. Qiu, L., Liu, F., Zhao, L., Ma, Y., and Yao, J., *Appl. Surf. Sci.,* 2006, vol. 252, pp. 4931–4935.
78. Masui, T., Fujiwara, K., Machida, K., and Adachi, G., *Chem. Mater*., 1997, vol. 9, pp. 2197–2204.
79. Tsunekawa, S., Fukuda, T., and Kasuya, A., *J. Appl. Phys*., 2000, vol. 87, pp. 1318–1321.
80. Nie, J.C., Hua, Z.Y., Dou, R.F., and Tu, Q.T., *J. Appl. Phys*., 2008, vol. 103, pp. 054308-1–054308-7.
81. Ivanov, V.K., Polezhaeva, O.S., Kopitsa, G.P., Baranchikov, A.E., and Tret'yakov, Yu.D., *Neorg. Mater*., 2008, vol. 44, no. 3, pp. 324–330.
82. Yin, L., Wang, Y., Pang, G., Koltypin, Yu., and Gedanken, A., *J. Coll. Int. Sci*., 2002, vol. 246, pp. 78–84.
83. Serpone, N., Dondi, D., and Albini, A., *Inorg. Chim. Acta*, 2007, vol. 360, pp. 794–802.
84. Linsebigler, A.L., Lu, G.Q., and Yates, J.T., *Chem. Rev*., 1995, vol. 95, pp. 735–738.
85. Herrmann, J.M., *Catal. Today*, 1999, vol. 53, pp. 115–129.
86. Dunford, R., Salinaro, A., Cai, L., Serpone, N., Horikoshi, S., Hidaka, H., and Knowland, J., *FEBS Lett*., 1997, vol. 418, pp. 87–90.
87. Wamer, W.G., Yin, J.-J., and Wei, R.R., *Free Radical Biol. Med*., 1997, vol. 23, pp. 851–858.
88. Li, R., Yabe, S., Yamashita, M., Momose, S., Yoshida, S., Yin, S., and Sato, T., *Mater. Chem. Phys*., 2002, vol. 75, pp. 39–44.
89. Li, R., Yabe, S., Yamashita, M., Momose, S., Yoshida, S., Yin, S., and Sato, T., *Solid State Ionics*, 2002, vol. 151, pp. 235–241.
90. Yamashita, M., Kameyama, K., Yabe, S., Yoshida, S., Fujishiro, Y., Kawai, T., and Sato, T., *J. Mater. Sci.,* 2002, vol. 37, pp. 683–687.
91. Yabe, S. and Sato, T., *J. Solid State Chem*., 2003, vol. 171, pp. 7–11.
92. Sato, T., Katakura, T., Yin, S., Fujimoto, T., and Yabe, S., *Solid State Ionics*, 2004, vol. 172, pp. 377–382.
93. El-Toni, A.M., Yin, S., Hayasaka, Y., and Sato, T., *J. Mater. Chem*., 2005, vol. 15, pp. 1293–1297.
94. El-Toni, A.M., Yin, S., Yabe, S., and Sato, T., *Mater. Res. Bull*., 2005, vol. 40, pp. 1059–1064.
95. El-Toni, A.M., Yin, S., Hayasaka, Y., and Sato, T., *J. Electroceram*., 2006, vol. 17, pp. 9–14.
96. Jakupec, M.A., Unfried, P., and Keppler, B.K., *Rev. Physiol. Biochem. Pharm*., 2005, vol. 153, pp. 101–111.
97. Schubert, D., Dargusch, R., Raitano, J., and Chan, S.-W., *Biochem. Biophys. Res. Comm*., 2006, vol. 342, pp. 86–91.
98. Das, M., Patil, S., Bhargava, N., Kang, J.-F., Riedel, L.M., Seal, S., and Hickman, J.J., *Biomat*., 2007, vol. 28, pp. 1918–1925.
99. Chen, J., Patil, S., Seal, S., and McGinnis, J.F., *Nature Nanotechnol*., 2006, vol. 1, pp. 142–150.
100. Rzigalinski, B.A., *Technol. Cancer Res. Treat*., 2005, vol. 4, pp. 651–659.
101. Ivanov, V.K., Fedotov, G.N., Nikulina M.V., Polezhaeva, O.S., Omel'yanyuk, G.G., Romanenko, S.N., Korol', S.G., and Tret'yakov, Yu.D., *Dokl. Ross. Akad. Nauk, Ser. Khim*., 2008, vol. 420, no. 5, pp. 628–631.
102. Baudry, P., Rodrigues, A.C.M., Aegerter, M.A., and Bulhoes, L.O., *J. Non-Cryst. Solids*, 1990, vol. 121, pp. 319–322.
103. Keomany, D., Poinsignon, C., and Deroo, D., *Sol. Energy Mater. Sol. Cells*, 1994, vol. 33, pp. 429–441.
104. Keomany, D., Petit, J.-P., and Deroo, D., *Sol. Energy Mater. Sol. Cells*, 1995, vol. 36, pp. 397–408.
105. Verma, A., Samanta, S.B., Bakshi, A.K., and Agnihotry, S.A., *Solid State Ionics*, 2004, vol. 171, pp. 81–90.
106. Orel, Z. C. and Orel, B., *SPIE Proc*., 1994, vol. 2255, pp. 285–296.
107. Huggins, R.A., *Ionics,* 1997, vol. 3, pp. 245–255.
108. Berton, M.A.C., Avellaneda, C.O., and Bulhoes, L.O.S., *Sol. Energy Mater. Sol. Cells*, 2003, vol. 80, pp. 443–449.
109. Zhu, B., Luo, Z., and Xia, C., *Mater. Res. Bull*., 1999, vol. 34, pp. 1507–1512.
110. Veszelei, M., Kullman, L., Azens, A., Granqvist, C.G., and Hjorvarsson, B., *J. Appl. Phys*., 1997, vol. 81, pp. 2024–2026.
111. Kullman, L., Veszelei, M., Ragan, D.D., Isidorsson, J., Vaivars, G., Kanders, U., Azens, A., Schelle, S., Hjorvarsson, B., and Granqvist, C.G., *SPIE Proc.,* 1996, vol. 2968, pp. 219–224.

112. Varsano, F., Decker, F., Masetti, E., Cardellini, F., and Licciulli, A., *Electrochim. Acta*, 1999, vol. 44, pp. 3149–3156.

113. Richards, B.S., *Progr. Photovolt: Res. Appl*., 2004, vol. 12, pp. 253–281.

114. Huang, D., Qin, F., Yao, Z., Ren, Z., Lim, L., Gao, W., and Ren, Q., *Appl. Phys. Lett*., 1995, vol. 67, pp. 3724–3725.

115. Inoue, T., Yamamoto, Y., Koyama, S., Suzuki, S., and Ueda, Y., *Appl. Phys. Lett*., 1995, vol. 56, pp. 1332–1333.

116. Corma, A., Atienzar, P., Garcia, H., and Chane-Ching, Y.-Y., *Nat. Mater*., 2004, vol. 3, pp. 394–397.

117. Lira-Cantu, M. and Krebs, F.C., *Sol. Energy Mater. Sol. Cells*, 2006, vol. 90, pp. 2076–2086.